Microporous and Mesoporous Materials 366 (2024) 112943

Investigation of mesoporous silicon thermal conductivity: Effect of nanographene insertion

Sibel Nar [a,b,c], Andrzej Kusiak [d], Rubenson Mareus [a], Arnaud Stolz [a], Denis Machon [b,e], Amaël Caillard [a], Jean-Luc Battaglia [d], Abderraouf Boucherif [b,c,**], Nadjib Semmar [a,*]

[a] Groupe de Recherches sur l'Énergétique des Milieux Ionisés (GREMI) – CNRS UMR 7344, Université d'Orléans, 14 Rue d'Issoudun, BP 6744, 45067, Orleans Cedex, France
[b] Laboratoire Nanotechnologies et Nanosystèmes (LN2) - CNRS IRL-3463, Université de Sherbrooke, 3000 Boulevard de l'Université, Sherbrooke, Québec, J1K OA5, Canada
[c] Institut Interdisciplinaire d'Innovation Technologique (3IT), Université de Sherbrooke, 3000 Boulevard de l'Université, Sherbrooke, J1K 0A5, QC, Canada
[d] Laboratory Trefle, UMR 8508, University of Bordeaux, 33405, Talence Cedex, France
[e] Université de Lyon, INSA Lyon, CNRS, École Centrale de Lyon, Université Claude Bernard Lyon 1, CPE Lyon, INL, UMR5270, 69621, Villeurbanne, France

Keywords:
Mesoporous silicon
Nanographene insertion
Nanocomposite
Thermal conductivity
Photothermal radiometry
ZT-Meter

A B S T R A C T

In this study, the impact of nanographene incorporation on the thermal properties of mesoporous silicon (PSi) was evaluated using two complementary experimental methods: the temperature gradient (TG) and the photothermal radiometry (MPTR) methods. It is shown that the measured thermal conductivity of the mesoporous silicon (PSi) ranges from 0.10 to 0.68 W/m.K in the case of TG and from 0.37 to 3.02 W/m.K in MPTR and is strongly correlated to the electrochemical etching parameters. These values are much lower than that of crystalline silicon, estimated to be from 100 to 140 W/m.K, depending on the doping rate. They appear to be, however, in the order of magnitude range for the percolation models that also include the in-depth porosity and the crystallite mean radius. This set of experiments on the thermal conductivity was extended to investigate the effect of graphene incorporation in the PSi matrix (G-PSi) as it has seldom been reported in the literature. The results from both methods exhibit significantly higher values (1.7 ± 0.3 W/m.K for TG, and from 0.7 to 2.13 W/m.K for MPTR). This spread of the thermal conductivity values is attributed to the intrinsic working principle of the TG versus the MPTR method as highlighted in the last part of the present paper. Targeting the thermoelectric application of both matrices (PSi, G-PSi), the thermal conductivity remains sufficiently low for them to be considered as very promising materials, keeping in mind the enhancement of the power-factor attributed to the incorporation of graphene.

1. Introduction

Silicon is an essential semi-conductor material in the field of microelectronics thanks to its properties, particularly electrical [1]. Recently, research has focused on the use of abundant semiconductor materials such as silicon for thermoelectric applications with a view to energy harvesting. A good thermoelectric material is characterized by a maximum figure of merit $ZT = \sigma S^2/kT$ with S, the Seebeck coefficient, σ the electrical conductivity, k the thermal conductivity and T the absolute temperature. In our recent work, we investigated the synthesis and characterization of mesoporous silicon and the effect of nanographene on the Seebeck coefficient [2]. In the present study, we focus on the thermal conductivity of these same materials to evaluate the effect of the insertion of nanographene on the thermal properties of mesoporous silicon. As reported in the thesis work of Nar S. [3], this carbon incorporation led to a clear improvement in the power factor ($PF = \sigma S^2$) of the nanographenized porous material from 60 to 250 μW/m.K^2. A similar result could be expected for the ZT after analyzing the thermal conductivity. Mesoporous silicon (PSi) obtained by the electrochemical etching of p or p + doped crystalline silicon is particularly interesting

* Corresponding author. Groupe de Recherches sur l'Énergétique des Milieux Ionisés (GREMI) – CNRS UMR 7344, Université d'Orléans, 14 Rue d'Issoudun, BP 6744, 45067, Orleans Cedex, France.
** Corresponding author. Laboratoire Nanotechnologies et Nanosystèmes (LN2) - CNRS IRL-3463, Universitè de Sherbrooke, 3000 Boulevard de l'Université, Sherbrooke, Québec, J1K OA5, Canada.
E-mail addresses: abderraouf.boucherif@usherbrooke.ca (A. Boucherif), nadjib.semmar@univ-orleans.fr (N. Semmar).

https://doi.org/10.1016/j.micromeso.2023.112943

Table 1
Porous Si thermal conductivity at room temperature.

Si wafer (type and resistivity)	Porosity (%)	Thickness (μm)	Thermal conductivity (W/m.K)	Measurement method	References
p	64	31–46	0.8 ± 0.1	3ω method	Gesele et al. [8]
0.2 Ω cm					
p+	50	10	2.5	Photoacoustic method	Benedetto et al. [18]
0.01 Ω cm	60	23	3.9		
p+	38	100	4.6	Micro-Raman	Lysenko et al. [9]
0.01 Ω cm	62		0.9		
	74		0.3		
p+	50	50	0.7	Micro-Raman	Périchon et al. [11]
0.02 Ω cm					
p+	55	26	1.93	Photoacoustic method	Amato et al. [10]
0.02 Ω cm	75		0.74		
p+	30	8	3.6	Scanning thermal microscopy	Gomes et al. [15]
0.01 Ω cm	54		2.2		
	80		1.4		
n	28	0.2	8.0 ± 0.8	Photothermal pulsed method	Melhem et al. [19]
0.01–0.015 Ω cm	32	1	7.0 ± 0.4		
	34	10	7.0 ± 0.7		
	41	50	5.0 ± 0.5		
n	20	100	5	Micro-Raman	Siegert et al. [20]
0.01 Ω cm			4.2	Electrothermal finite element	
p+	70	40	0.6	Direct current & Finite Element Method	Valalaki et al. [21,22]
1–10 Ω cm					

because of the ability to tailor its different properties (optical, electrical, and thermal) using controllable parameters such as thickness and porosity [1,4]. Interesting thermal insulation properties for these materials have already been reported in various works [4,5] specifically by the 3ω method. The thermal conductivity of bulk silicon is about 150 W/m.K for doping around 10^{18} - 10^{19} cm^{-3} and can be around 140 W/m.K for higher doping (10^{20} cm^{-3}) [6]. Values lying in the range 0.1–20 W/m.K have been measured for mesoporous silicon depending on the porosity, the thickness of the porous layer and the measurement technique adopted [7–18]. This drastic decrease by 2–3 orders of magnitude of the thermal conductivity of the nanostructured PSi is of interest in the field of thermoelectricity since a good thermoelectric material must exhibit a low thermal conductivity. Table 1 summarizes the different methods used to determine the thermal conductivity of PSi as well as the characteristics of the initial substrate used and the morphological parameters of PSi.

The 3ω method is the one most commonly used for evaluating thermal properties. It requires depositing a metal strip on the sample surface to enable Joule heating of the studied material. Often, photolithography is used to perform this type of sample preparation. Gesele et al. [8] observed a value of 0.8 W/m.K at 300 K on mesoporous silicon with a thickness of 21 μm and a porosity of 64 % obtained by p + doped Si. For p-doped, they obtained a value of 0.2 W/m.K for the same porosity and 31 μm thickness. By increasing this porosity to 89 %, and the same thickness, for p-doped porous Si, they reached a value of 0.05 W/m.K with a 31 μm-thick layer. This indicates that both the porosity and thickness of the porous layer are critical parameters for thermal conductivity.

Raman spectroscopy is an alternative method to measure the local thermal conductivity of porous materials. Unlike the previous technique, it is non-destructive. Laser absorption induces local heating and by increasing the temperature one can determine the thermal conductivity. For instance, Lysenko et al. [9] used the micro-Raman technique to evaluate the thermal conductivity of a 100 μm porous layer obtained with a p + type substrate as a function of the porosity. They also observed a decrease in thermal conductivity with increasing porosity of the material, with a value of 0.3 W/m.K for 74 % porosity [9].

This effect of porosity is understandable as a porous material is composed of a solid matrix and air, which has a negligible thermal conductivity. Therefore, the thermal conductivity of a porous material can be approximated by weighting the thermal conductivity of Silicon by a factor of 1-P, where P represents the porosity. However, this approximation is not verified over the whole range of porosities. For example, for a porosity of 90 %, the thermal conductivity is not 10 times

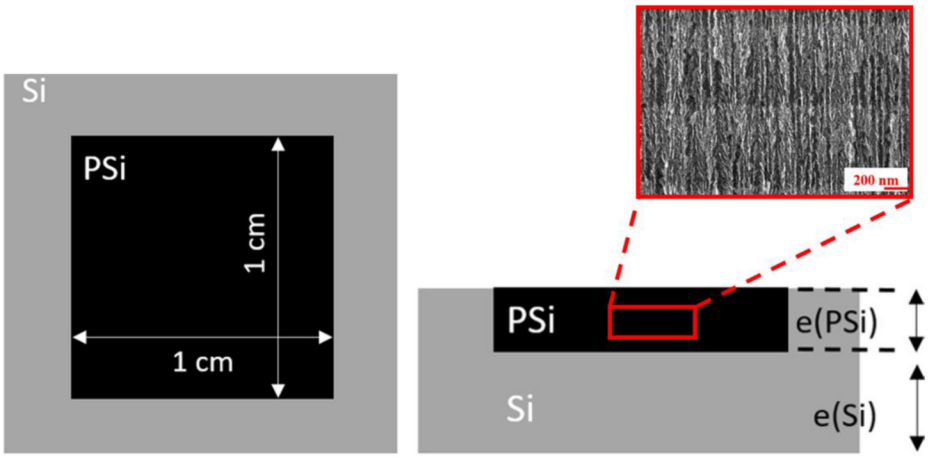

Fig. 1. – Geometry of the studied samples: top and cross view (grey = bulk silicon, black: mesoporous silicon). SEM image in insert represents a porous sample with e (PSi) = 60 μm of thickness on top of Si substrate of e(Si) = 440 μm.

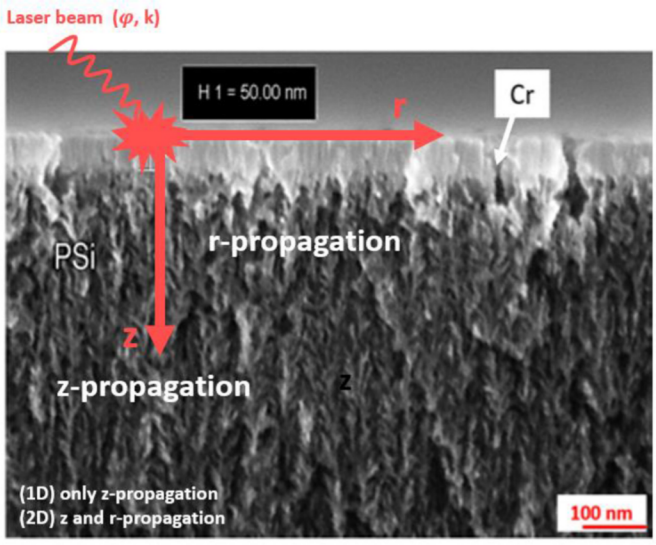

Fig. 2. SEM image of mesoporous Si with a layer of chromium on the top.

lower, as could be expected. Gesele et al. [8] and Lysenko et al. [9] set up a model that links the variation in the thermal conductivity of mesoporous silicon to other intrinsic parameters, leading to equation (1):

$$k_{PSi} = (1-P)^3 \times \frac{k_{Si}}{1+\frac{4}{3}\frac{\Lambda_{Si}}{r_{Cr}}} \quad (1)$$

where P is the porosity, k_{Si} the thermal conductivity of the bulk silicon, Λ_{Si} the mean free path of the phonons and r_{Cr} is the mean radius of the crystallites forming the porous silicon. The cubed power of the factor 1-P describes the percolation in the material [8]. The crystallite size is about 10 nm for mesoporous silicon [8]. As for the mean free path in bulk silicon, at room temperature, it takes the value of 43 nm [22]. The thermal conductivity of nanostructured silicon is therefore drastically lower than that of bulk silicon thanks to the porosity and the average radius of the crystallites forming the porous material.

2. Materials synthesis

The synthesis of materials is described in Ref. [2]. The samples are made of p + type boron doped (100)-oriented silicon (Si) wafers (resistivity <0.005 Ω cm) (WaferPro, Santa Clara, CA, USA) on which a section has been electrochemically etched (Fig. 1). Four different thicknesses of the mesoporous silicon layer e(PSi) (30, 50, 60 and 150 μm) were selected for mesoporous silicon, Psi, and nanographene-coated mesoporous silicon, G-PSi, of assumed identical porosity (50 %) for a current density fixed at 100 mA/cm^2.

Each sample was coated with 50 nm of chromium (Cr), acting as an optical-thermal transducer for photothermal measurements. The transducer layer protects the mesoporous material and given its high extinction coefficient (4.07 Ref. [23]) ensures absorption of the laser beam, thus preventing its propagation into the porous material. On the other hand, its thickness is low enough (50 nm) to consider that this metallic layer is uniformly thermalized during thermal measurements. The Cr layers were deposited at room temperature on p + doped porosified silicon (100) by magnetron sputtering. The Cr target is a metal disc 101.6 mm in diameter of pure chromium (99.9 % purity), located 10 cm from the substrate holder. Before deposition, the samples underwent deoxidation carried out in a hydrofluoric acid-ethanol mixture for a few minutes. The deposition was operated at constant power (100 W) in a plasma discharge formed of Ar. The gas was introduced into the chamber by a mass flow regulator. A gas flow of 20 sccm was used, which corresponds to an argon working pressure of 0.3 Pa. A

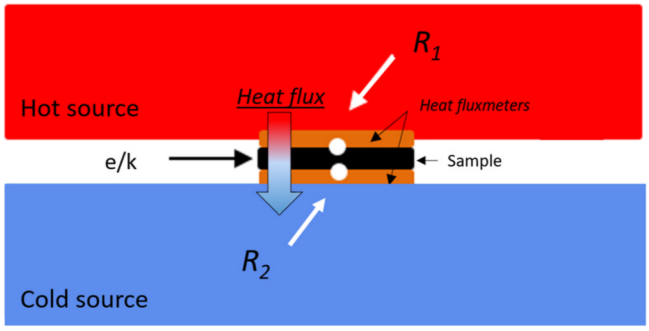

Fig. 3. Illustration of thermal measurement via ZT-meter fully described in Ref. [2]. Red and blue blocks are respectively the hot and the cold part of the device to create the heat flux. The sample is shown in black and encircled by heat fluxmeters.

SEM cross section image of the PSi with Cr transducer is shown in Fig. 2.

3. Measurement of thermal properties

3.1. Temperature gradient (TG) method by ZT-meter

The ZT-meter used in this study is that described in Ref. [2]. This device is home-made at GREMI, and is used to perform simultaneous measurements of thermal conductivity and the Seebeck coefficient. In Ref. [2], the ZT-meter is described for Seebeck coefficient measurements. In order to measure the thermal properties, fluxmeters are present, thus allowing the heat flux generated by the temperature difference between the hot and cold blocks to be measured. The sensitivity of each heat fluxmeter allows the heat flux to be determined from the voltage delivered by the fluxmeter. The measurement principle is illustrated in Fig. 3.

The temperature difference ΔT between the hot and cold blocks can be written according to Fourier's law (equation (2)):

$$\Delta T = \varphi\left[R_1 + R_2 + \frac{e}{k}\right] \quad (2)$$

where Φ is the heat flux, R_1 and R_2 the contact resistances, e the material thickness and k the thermal conductivity of the material.

The thermal flux is determined by converting:

$$\varphi = \frac{V}{S_e} \quad (3)$$

where V is the voltage measured and S_e the sensitivity of the fluxmeter, S_e (hot side) = 0.473 μV/(W/m^2) and S_e (cold side) = 0.453 μV/(W/m^2).

In the case of porous materials such as mesoporous silicon, the contact resistances are difficult to evaluate. An estimate can be made using a highly conductive material as a reference. Copper is a good thermal conductor with a thermal conductivity of k_{Cu} = 400 W/m.K [24]. To estimate the contact resistances, we therefore used a very thin copper sample with e_{Cu} = 450 μm in order to neglect the contribution of this component in equation (2) leading to:

$$\Delta T = \varphi[R_1 + R_2] \quad (4)$$

Experimentally, obtaining a straight line of the form ΔT = a Φ with a = R_1+R_2 as a slope would make it possible to deduce the contact resistances with copper or bulk silicon. This value will be used to determine the thermal conductivity of coated or uncoated mesoporous silicon, PSi and G-PSi, respectively.

These thermal conductivities can be determined as:

$$k = \frac{e}{R - (R_1 + R_2)} \quad (5)$$

where R_1 and R_2 are the contact resistances for copper and R is the

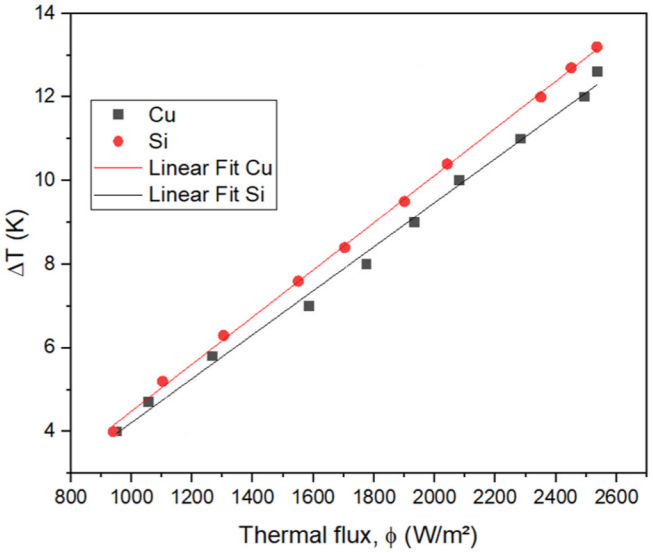

Fig. 4. – Temperature difference between the cold and hot blocks vs the thermal flux. Thermal resistance for Cu and Si bulk.

Table 2
Thermal conductivity of PSi obtained by using the thermal contact resistances from Cu and Si.

	Thickness (m)	R (m^2.K/W)	k (Si (R_1+R_2)) (W/m.K)	k (Cu (R_1+R_2)) (W/m.K)
PSi-2	3×10^{-5}	53.1×10^{-4}	0.32	0.68
PSi-3	5×10^{-5}	53.8×10^{-4}	0.29	0.41
PSi-5	6×10^{-5}	54.3×10^{-4}	0.27	0.34
PSi-9	1.5×10^{-4}	66.6×10^{-4}	0.10	0.10

Table 3
Thermal conductivity of PSi and G-PSi.

Thickness of mesoporous layer (μm)	k (W/m.K)	Δk/k (%)
30 (PSi-2)	0.68	37
50 (PSi-3)	0.41	30
60 (PSi-5)	0.34	23
150 (PSi-9)	0.10	9
30 (G-PSi-2)	1.91	95
50 (G-PSi-3)	1.47	85
60 (G-PSi-5)	1.68	70
150 (G-PSi-9)	1.56	82

between ΔT and φ (Fig. 4).

Fig. 4 shows the relation $\Delta T = R.\varphi$. R is $(52.6 \pm 1) \times 10^{-4}$ m^2 K/W for Cu and $(52.1 \pm 1) \times 10^{-4}$ m^2 K/W for Si, respectively. In the case of Bi_2Te_3, a reference material in thermoelectricity and for this method, the thermal conductivity determined is 1.85 ± 0.15 W/m.K and 1.80 W/m.K. This value is quite consistent with the values found in the literature for Bi_2Te_3 [22,24–26], which range from 1 to 3 W/m.K. The same methodology was used to determine the thermal conductivity of mesoporous silicon. Table 2 summarizes the values of slopes, the thermal conductivity and the associated uncertainties for PSi.

The thermal conductivities determined by estimating the contact resistances with Si show very low values, in contrast to the conductivities measured for this type of PSi (equivalent thickness) in the literature. The thermal conductivities obtained by estimating the contact resistances with copper are twice as high for PSi-2 and identical for the PSi-9 sample. In the following, we decided to determine k using the contact resistances estimated from the slopes obtained with copper (k (Cu) ≫ k(Si)). Results are illustrated in Table 3 with Δk/k uncertainties for each material directly deduced by the formula given in the Appendices section.

Lysenko et al. [10] measured a thermal conductivity of 0.3 W/m K by the micro-Raman technique on a p + doped PSi substrate with a porosity of 74 %. Valalaki et al. [16] determined by FEM simulation a value two times higher, k = 0.6 W/m.K for a p + doped PSi with a 70 % porosity, suggesting a slight effect of dopant material. For a porosity of 64 %, Gesele et al. [8] measured a thermal conductivity of 0.8 W/m.K on a p-doped Si substrate by the 3ω method. In our case, i.e. a porosity of PSi substrates with different thicknesses estimated at 50 %, the conductivities ranged from 0.10 to 0.68 W/m.K, which seems consistent with the literature values. More specifically, for PSi-3 the k value is 0.4 W/m.K. For these same conditions (p + doping, porosity and thickness), Périchon et al. measured a conductivity of 0.7 W/m.K [11] by the micro-Raman technique. Depending on the type of substrate doping and the measurement configuration (in-plane, in-depth) used to determine the thermal conductivity, the values are slightly different, and remain in all cases very low compared to the c-Si values even with the percolation method. An evaluation of the thermal properties on G-PSi is completely lacking in the literature. We will therefore refer to those of PSi to compare and explain the thermal conductivities measured on this graphene-based nanocomposite. As expected from the literature, the insertion of nanographene affects the thermal conduction [27]: the measured thermal conductivity of all G-PSi samples was higher than that of PSi. The values ranged from 1.47 to 1.91 W/m.K with higher measurement uncertainties as summarized in Table 3. To complete this thermal conductivity investigation a second measurement technique was employed to obtain a second set of values on the same PSi and GPSi samples. The MPTR (Modulated Photothermal Radiometry) method is known to be a powerful technique for the thermal characterization of coatings and thin films [28,29]. The results obtained are reported in the following section.

3.2. *Modulated photothermal radiometry (MPTR)*

Modulated photothermal radiometry is a measurement technique based on the detection of infrared radiation emitted by a surface in response to a photothermal excitation. This method is largely described in the literature [28,30,31]. Generally, a laser source is used to produce the modulated thermal excitation. Following absorption of the laser beam on the sample surface, an infrared radiation (IR) is emitted, in accordance with the Stefan-Boltzmann law. This self-emission is considered linearly linked to the temperature when temperature variation is low.

The schematic view of the experimental MPTR setup used in this work is presented in Fig. 5 and detailed in Refs. [28,30,31]. The thermal perturbation of the characterized sample is generated by a 1064 nm wavelength CW laser with 1.7 W maximum power. The Gaussian laser spot at the sample surface is 0.75 mm in radius. Laser modulation is accomplished using an acousto-optic modulator according to a square signal of frequency supplied by a function generator. A fast, 2 ns rise time, InGaAs photodetector is used to follow the laser beam intensity in order to supply a reference signal and avoid any delay due to the acousto-optic modulator. The samples are placed in a heating device at the focal plane of a set of off-axis parabolic mirrors in order to collect the emitted IR radiation. The IR signal is measured by an HgCdTe infrared detector 1 mm in diameter. A lock-in amplifier is used to measure the amplitude and the phase lag between the IR detector signal and the photodetector reference as a function of frequency, since the phase lag will be used as an explanatory variable to estimate the PSi thermal conductivity. All the measurements are carried out at 35 °C fixed by the heating device on the rear face of the sample.

The representative parameters of the studied samples obtained from

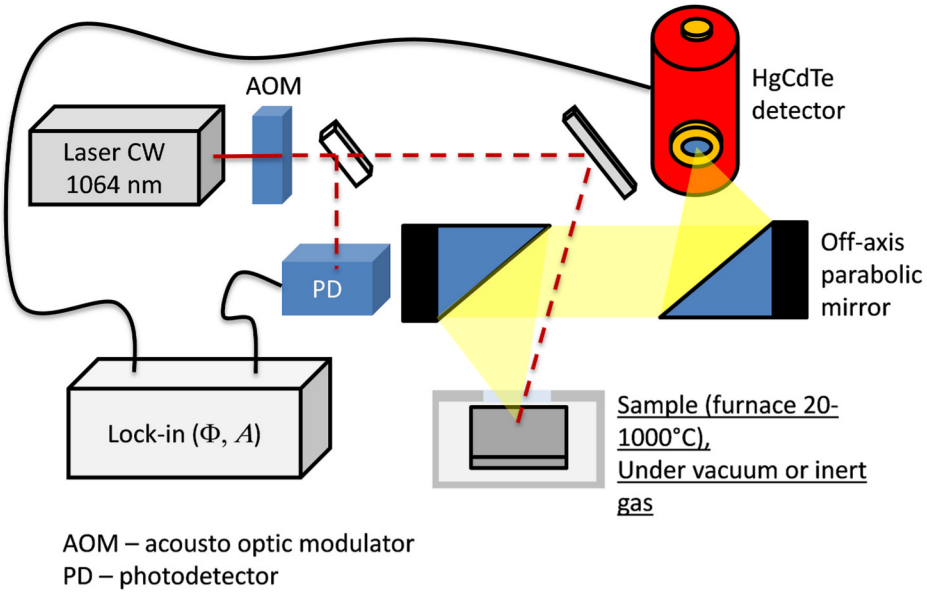

Fig. 5. – Schematic view of the MPTR setup used in the work.

Table 4
Set of parameters representative of the study and used for the phase calculation.

	Value	Reference/Source
Thickness of the silicon substrate (m)	[470, 450, 440 and 350] x 10^{-6}	Measured – sample preparation
Thickness of the mesoporous layer (m)	[30, 50, 60 and 150] x 10^{-6}	Measured – sample preparation
Thermal capacity of silicon (J.m^{-3}.K^{-1})	1.67 × 10^{6}	[32]
Thermal conductivity of silicon (W/m.K)	100–140	[32,33]
Thermal capacity of mesoporous silicon (J.m^{-3}.K^{-1})	1.26 × 10^{6}	[34]
Thermal conductivity of mesoporous silicon (W/m.K)	1	[8] [this work]
Radius of excitation r_0 (m)	0.75 × 10^{-3}	Measured – MPTR experimental configuration
Radius of measurement r_m (m)	0.5 × 10^{-3}	Measured – MPTR experimental configuration
Radius of sample R (m)	5 × 10^{-3}	Measured – MPTR experimental configuration

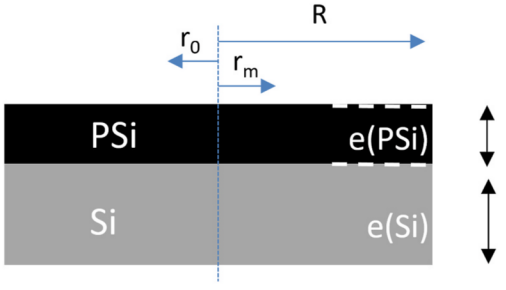

Fig. 6. - Approximation of the studied samples to a bilayer with R the radius of the sample, r0 the excitation radius and rm the measurement radius. The same is considered in the case of G-PSi.

the literature and those measured in the experiment are collected in Table 4. These data are used to select the MPTR measurement conditions. Firstly, given the extent of the PSi layer in the plane of the sample, the thermal diffusion length *d* is:

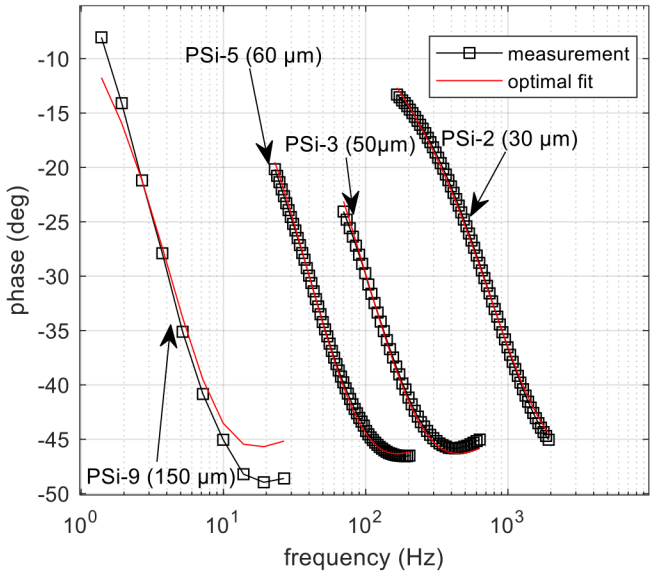

Fig. 7. - Estimation of the thermal conductivity of PSi: representations of the measured and calculated phases with the optimal value of the thermal conductivity for the different thicknesses: PSi-2, PSi-3, PSi-5 and PSi-9.

$$d = \sqrt{a/\pi f} \tag{6}$$

As this length, in the Si substrate, does not exceed 2 mm (the Si substrate has a larger thermal diffusivity *a* than the PSi layer) at the modulation frequency *f* of 10 Hz, the system can be viewed as a bilayer (see Fig. 6).

Secondly, in order to enable the estimation of the thermal conductivity of porous layers, a proper frequency range swept during measurement is selected. The maximum frequency is that leading to a semi-infinite behavior of the porous layer, i.e. corresponding to the thermal diffusion length equivalent to the layer thickness, as measurements at higher frequencies would not give information about the thermal properties of the layer. The minimum frequency value is chosen in order to cover at least a decade of frequencies. It should be noted that the swept frequency range must be adjusted according to the PSi thickness.

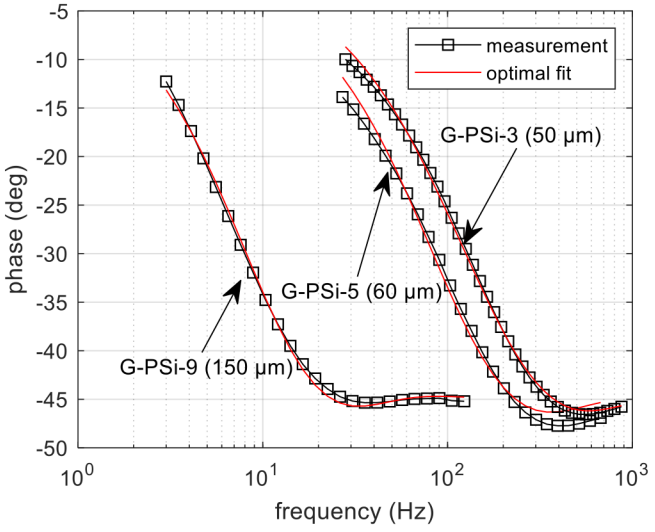

Fig. 8. - Estimation of the thermal conductivity of G-PSi: representations of the measured and calculated phases with the optimal value of the thermal conductivity for the different thicknesses: G-PSi-3, G-PSi-5 and G-PSi-9.

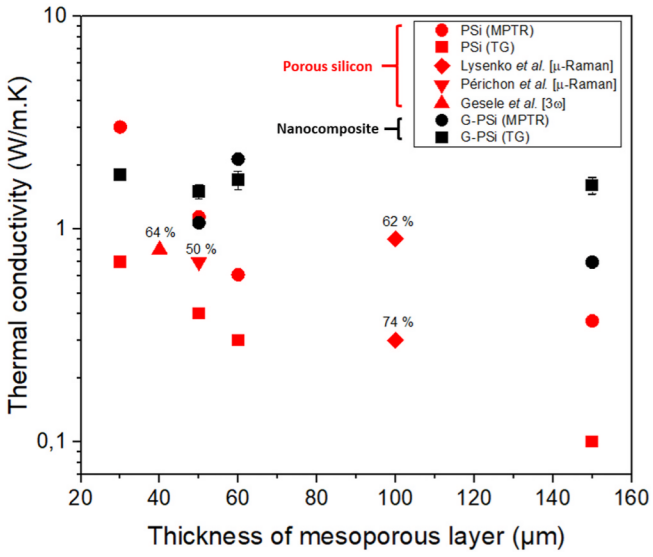

Fig. 9. - Thermal conductivities of PSi and G-PSI by two methods: TG method & MPTR. The thermal conductivities are compared to those obtained in the work of Gesele et al. [8], Lysenko et al. [9] and Périchon et al. [11]. The percentage values correspond to the porosities.

Table 5
Thermal conductivities of PSi and G-PSi determined by MPTR.

Thickness of mesoporous layer (µm)	Thermal conductivity (W/m.K)	Absolute error (W/m.K)	Δk/k (%)
30 (PSi-2)	3.02	0.10	3
50 (PSi-3)	1.14	0.08	7
60 (PSi-5)	0.61	0.09	15
150 (PSi-9)	0.37	0.13	35
50 (G-PSi-3)	1.07	0.11	10
60 (G-PSi-5)	2.13	0.17	8
150 (G-PSi-9)	0.70	0.15	21

Following this approach and using values from Table 4, the maximum frequency was found to be around 11 Hz for the thickest layer (150 µm) and around 300 Hz for the thinnest (30 µm) PSi. Low frequencies will be preferred for large porous thicknesses and higher frequencies for thinner layers. As the encountered measurement frequencies are low, axial symmetry regarding heating and measurement and thus in-plane and out of plane heat diffusion is considered even if isotropic thermal conductivity is assumed. Obviously, 1D heat transfer will appear for frequencies neighboring the semi-infinite behavior of the sample.

In the studied configuration, the MPTR measurements are sensitive to the thermal conductivity but also to the thermal capacity of the mesoporous silicon. In order to estimate the thermal conductivity of the studied samples, the thermal capacity of the PSi used here was that reported in Ref. [34].

3.2.1. Thermal conductivity determined by MPTR

The Levenberg-Marquardt algorithm is used to minimize the gap between experimentally measured and calculated thermal response, using the heat transfer model phase by adjusting the mesoporous layer thermal conductivity [29]. Figs. 7 and 8 show the measured and calculated phase with the optimal identified value of the mesoporous thermal conductivity for PSi and G-PSi, respectively.

The adjusted thermal conductivities as well as the uncertainty on each value for PSi and G-PSi are collected in Table 5. The thickness of the porous layer is taken as a reference since the increase in thickness creates more open porosities on the surface as shown in Ref. [2], and this implies that the porous material becomes more insulating.

The thermal conductivity values of porous silicon determined in previous studies are quite similar to those determined by MPTR. Gesele et al. [8] employed the 3ω method, a widely-used method for determining the thermal properties of materials. They probed a depth down to around 30 µm and showed that for mesoporous silicon with a thickness of 21 µm and a porosity of 64 %, the thermal conductivity was 0.8 W/m.K at 300 K. By increasing the porosity, they showed that the thermal conductivity decreased to 0.06 W/m.K for 71 % and 0.05 W/m.K for 89 % porosity. The samples studied in this work have porosities around 50 % so the higher thermal conductivity values for thicknesses of 30 and 50 µm are not surprising. The synthesis of thick layers can cause in-depth porosity gradients [35], which is why it is difficult to assert that our porosities are similar in-plane and in-depth. This could therefore explain, as in the case of the Seebeck coefficient [2,35], the variations in thermal conductivity with the etching time, making it possible to obtain increasingly thick layers.

In general, it can be expected that the insertion of nanographene contributes to the increase of the apparent thermal conductivity of the composite. However, in the present case, both methods (TG and MPTR) show a slight increase in the thermal conductivity of the G-PSi versus PSi. Since the deposit is nanographene with an intense D peak (presence of defects) and a low intensity 2D peak [2], we do not have the full thermal conduction properties of graphene.

These results on nanocomposites are therefore still very promising for future thermoelectric applications [2].

Both methods make it possible to determine the thermal conductivities measured for both materials PSi and G-Psi. The conductivity values are much lower than those of p + doped silicon substrates which have values of the order of 100–150 W/m.K. High uncertainties are obtained with the ZT-meter method, specifically for G-PSi, related to the conduction, which increases ($k > 1$ W/m.K) with the incorporation of nanographene. The method seems more suitable for insulating materials with values below 1 W/m.K. In Fig. 9, the values of k obtained with the two methods are compared with values reported in the literature [7,9,11].

From equation (6), the thermal diffusion length was calculated as a function of the modulation frequency. For this calculation, we used the specific heat and the density from a barycentric model thanks to a porosity value of 50 %. From this model, the specific heat of PSi (barycentric model) was estimated to be 0.83×10^6 J/m^3.K, which is close to the value proposed in Ref. [34]. For the sample PSi-3 (50 µm) that returns a k value of 1.14 W/m.K, the diffusion length ranges from 8 to

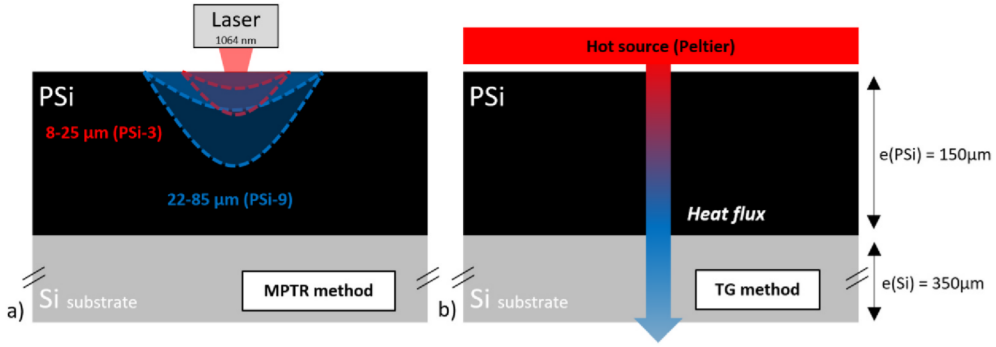

Fig. 10. Comparison of the two heat wave situations: (a) MPTR with the laser beam induced thermal length as a function of the modulation frequency, and (b) TG method with the heat wave passing through the whole material (PSi + Si).

25 µm corresponding to a frequency from 70 to 700 Hz. On the other hand, for the sample PSi-9 (150 µm), that returns a k value of 0.37 W/m.K, the diffusion length ranges from 22 to 85 µm corresponding to a frequency from 2 to 30 Hz (Figs. 7 and 10-a). Given that PSi-9 is a more insulating sample than PSi-3, the targeted frequency ranges are different. This difference in the diffusion lengths could explain the spread of the k values that are intrinsic to the 'probed' area with different chemical and morphological features, whereas in the TG method, the heat waves cross the entire substrate (PSi and Si) (Fig. 10-b).

These two different thermal scenarii explain why the thermal conductivities determined by MPTR are always higher than those determined by ZT-meter given that the porosity and the chemical changes induced are more predominant in the subsurface area than on the whole mesoporous layer [2].

In the case of carbonaceous materials, we also measured for each G-PSi a higher thermal conductivity compared to PSi. In fact, the incorporation of graphene also affects the thermal properties of the materials. Recent work by Pradhan et al. [27] showed that the incorporation of graphene into aluminum increased the thermal conductivity 2.3-fold (120 W/m.K for Al to 280 W/m.K for Al-Graphene), determined by an indirect method measuring the thermal diffusivity of materials (Linseis XFA 600, Germany). The MPTR and TG methods also gave higher thermal conductivity values in the case of graphenized samples, as reported in Tables 3 and 5 However, on increasing the thermal diffusion throughout the PSi and Si substrates, the measurement uncertainties also increase more significantly when using the TG method, exceeding the metrology limits of this measurement technique.

4. Conclusion

In this work, we have demonstrated the successful measurement of thermal conductivity on electrochemical etched silicon (PSi) and a graphene-incorporated mesoporous matrix (G-PSi). Two experimental methods, the temperature gradient method (TG option of the ZT-meter device) and modulated photothermal radiometry, were used to investigate in depth the thermal conductivity behavior versus the etching time for each selected method, as well as the spread of values which depends on the experimental method used. For the PSi substrates, the conductivity values are quite similar to those reported in the different references on the mesoporous state. The thermal properties of the G-PSi samples, rarely reported in the literature, showed systematically higher values versus the PSi case but remain at a very low level compared to the c-Si substrate. For this composite case, the TG method seems unsuitable to investigate the G-PSi substrate (and higher conductivity cases) due to a level of uncertainties close to 70 %. It can however be concluded that the ZT-meter device (already used for determination of the Seebeck coefficient in Ref. [2]) is suitable for the determination of thermal conductivity of insulating materials such as mesoporous silicon, as uncertainties did not exceed 30 %.

CRediT authorship contribution statement

Sibel Nar: Writing – review & editing, Writing – original draft, Visualization, Validation, Methodology, Investigation, Formal analysis, Data curation, Conceptualization. **Andrzej Kusiak:** Writing – review & editing, Visualization, Validation, Methodology, Investigation. **Rubenson Mareus:** Methodology, Investigation. **Arnaud Stolz:** Writing – review & editing, Validation, Supervision, Software, Methodology, Investigation, Conceptualization. **Denis Machon:** Writing – review & editing, Visualization, Validation, Supervision, Methodology, Investigation, Conceptualization. **Amaël Caillard:** Methodology, Investigation. **Jean-Luc Battaglia:** Software, Methodology, Investigation. **Abderraouf Boucherif:** Project administration, Funding acquisition, Conceptualization. **Nadjib Semmar:** Writing – review & editing, Writing – original draft, Visualization, Validation, Supervision, Resources, Project administration, Methodology, Funding acquisition, Conceptualization.

Declaration of competing interest

The authors declare that they have no known competing financial interests or personal relationships that could have appeared to influence the work reported in this paper.

Data availability

Data will be made available on request.

Acknowledgements

LN2 is a joint International Research Laboratory (IRL 3463) funded and co-operated in Canada by the Université de Sherbrooke (UdeS) and in France by CNRS as well as ECL, INSA Lyon, and Université Grenoble Alpes (UGA). It is also supported by the Fonds de Recherche du Québec Nature et Technologie (FRQNT). Boucherif would like to thank NSERC for the Discovery Grant for financial support. The Authors would like to thank the University of Orléans and the University of Sherbrooke for their support through a thesis grant and the Renatech network for supporting the cleanroom facilities.

Appendices

Determination of uncertainties on k determined by the temperature gradient method

$$\frac{\Delta k}{k} = \frac{\Delta e}{e} + \frac{\Delta R}{R} + \frac{\Delta(R_1 + R_2)}{R_1 + R_2}$$

$$\frac{\Delta(R_1 + R_2)}{R_1 + R_2} = \frac{\Delta\varphi}{\varphi} + \frac{\Delta T}{T}$$

with e, the thickness of the material (μm), and R the thermal resistance of the material (Bi_2Te_3 or PSi) (m^2.K/W). R_1+R_2 is the thermal resistance of Cu estimated by linear fit of $\Delta T = f(\Phi)$ (m^2.K/W).

References

[1] W. Theiß, Optical properties of porous silicon, Surf. Sci. Rep. 29 (1997) 91–192, https://doi.org/10.1016/S0167-5729(96)00012-X.

[2] S. Nar, A. Stolz, D. Machon, E. Bourhis, P. Andreazza, A. Boucherif, N. Semmar, Effect of nanographene coating on the Seebeck coefficient of mesoporous silicon, Nanomaterials 13 (2023) 1254, https://doi.org/10.3390/nano13071254.

[3] S. Nar, « Synthèse, caractérisation physico-chimique et propriétés thermoélectriques du silicium mésoporeux : apport de l'insertion de nanographène », Thesis, Sciences et Technologies Industrielles, Orléans, Université d'Orléans, 2023.

[4] S. Perichon, V. Lysenko, B. Remaki, D. Barbier, B. Champagnon, Measurement of porous silicon thermal conductivity by micro-Raman scattering, J. Appl. Phys. 86 (1999) 4700–4702, https://doi.org/10.1063/1.371424.

[5] A.S. Fedorov, A.S. Teplinskaia, Thermal properties of porous silicon nanomaterials, Materials 15 (2022) 8678, https://doi.org/10.3390/ma15238678.

[6] Y. Lee, Y, G.S. Hwang, Mechanism of thermal conductivity suppression in doped silicon studied with nonequilibrium molecular dynamics, Phys. Rev. B 86 (2012), 075202, https://doi.org/10.1103/PhysRevB.86.075202.

[7] A. Drost, P. Steiner, H. Moser, W. Lang, Thermal conductivity of porous silicon, Sensor. Mater. 7 (1995) 111–120.

[8] G. Gesele, J. Linsmeier, V. Drach, J. Fricke, R. Arens-Fischer, Temperature-dependent thermal conductivity of porous silicon, J. Phys. D Appl. Phys. 30 (1997) 2911–2916, https://doi.org/10.1088/0022-3727/30/21/001.

[9] V. Lysenko, S. Perichon, B. Remaki, D. Barbier, B. Champagnon, Thermal conductivity of thick meso-porous silicon layers by micro-Raman scattering, J. Appl. Phys. 86 (1999) 6841–6846, https://doi.org/10.1063/1.371760.

[10] G. Amato, R. Angelucci, G. Benedetto, L. Boarino, L. Dori, P. Maccagnani, A. M. Rossi, R. Spagnolo, Thermal characterisation of porous silicon membranes, J. Porous Mater. 7 (2000) 183–186, https://doi.org/10.1023/A:1009630619528.

[11] S. Perichon, V. Lysenko, P. Roussel, B. Remaki, B. Champagnon, D. Barbier, P. Pinard, Technology and micro-Raman characterization of thick meso-porous silicon layers for thermal effect microsystems, Sens. Actuator A-Phys. 85 (2000) 335–339, https://doi.org/10.1016/S0924-4247(00)00327-7.

[12] U. Bernini, R. Bernini, P. Maddalena, E. Massera, P. Rucco, Determination of thermal diffusivity of suspended porous silicon films by thermal lens technique, Appl. Phys. A 81 (2005) 399–404, https://doi.org/10.1007/s00339-004-2601-6.

[13] S. Lettieri, U. Bernini, E. Massera, P. Maddalena, Optical investigations on thermal conductivity in n- and p-type porous silicon, Phys. Status Solidi 2 (2005) 3414–3418, https://doi.org/10.1002/pssc.200461194.

[14] T. Kihara, T. Harada, N. Koshida, Precise thermal characterization of confined nanocrystalline silicon by 3ω method, Jpn. J. Appl. Phys. 44 (2005) 4084–4087, https://doi.org/10.1143/JJAP.44.4084.

[15] S. Gomès, L. David, V. Lysenko, A. Descamps, T. Nychyporuk, Application of scanning thermal microscopy for thermal conductivity measurements on meso-porous silicon thin films, J. Phys. D Appl. Phys. 40 (2007) 6677–6683, https://doi.org/10.1088/0022-3727/40/21/029.

[16] A. Wolf, R. Brendel, Thermal conductivity of sintered porous silicon films, Thin Solid Films 513 (2006) 385–390, https://doi.org/10.1016/j.tsf.2006.01.073.

[17] G. Chen, Nonlocal and nonequilibrium heat conduction in the vicinity of nanoparticles, J. Heat Tran. 118 (1996) 539–545, https://doi.org/10.1115/1.2822665.

[18] G. Benedetto, L. Boarino, R. Spagnolo, Evaluation of thermal conductivity of porous silicon layers by a photoacoustic method, Appl. Phys. A 64 (1997) 155–159, https://doi.org/10.1007/s003390050457.

[19] A. Melhem, D.S. Meneses, C. Andreazza-Vignolles, T. Defforge, G. Gautier, N. Semmar, Structural, optical, and thermal analysis of n-type mesoporous silicon prepared by electrochemical etching, J. Phys. Chem. C 119 (2015) 21443–21451, https://doi.org/10.1021/acs.jpcc.5b04984.

[20] L. Siegert, M. Capelle, F. Roqueta, V. Lysenko, G. Gautier, Evaluation of mesoporous silicon thermal conductivity by electrothermal finite element simulation, Nanoscale Res. Lett. 7 (2012) 427, https://doi.org/10.1186/1556-276X-7-427.

[21] K. Valalaki, A.G. Nassiopoulou, Porous Silicon as an Efficient Local Thermal Isolation Platform on the Si Wafer in the Temperature Range 5–350K, 11th International Workshop on Low Temperature Electronics, Grenoble, 2014, pp. 61–64, https://doi.org/10.1109/WOLTE.2014.6881026. France.

[22] A. Valalaki, « Etude des propriétés thermoélectriques et d'isolation thermique de Si poreux et Si nanocristallin », Thesis, Nanoelectronics and Nanotechnologies, University of Grenoble Alpes, Grenoble, 2006.

[23] A.D. Rakic, A.B. Djurisic, J.M. Elazar, M.L. Majewski, Optical properties of metallic films for vertical-cavity optoelectronic devices, Appl. Opt. 37 (1998) 5271–5283, https://doi.org/10.1364/AO.37.005271.

[24] M.J. Goglia, G.A. Hawkins, J.E. Deverall, Determination of thermal conductivity of copper and deoxidized copper-iron alloys, Anal. Chem. 24 (1952) 493–496, https://doi.org/10.1021/ac60063a016.

[25] T. Plecháček, J. Navrátil, J. Horák, P. Lošťák, Defect structure of Pb-doped Bi_2Te_3 single crystals, Philos. Mag. A 84 (2004) 2217–2228, https://doi.org/10.1080/14786430410001678226.

[26] D.L. Greenaway, G. Harbeke, Band structure of bismuth telluride, bismuth selenide and their respective alloys, J. Phys. Chem. Solid. 26 (1965) 1585–1604, https://doi.org/10.1016/0022-3697(65)90092-2.

[27] S.K. Pradhan, M.R. Sahoo, S. Ratha, B. Polai, A. Mitra, B. Sathpathy, A. Sahu, S. Kar, P.V. Satyam, P.M. Ajayan, S.K. Nayak, Graphene-incorporated aluminum with enhanced thermal and mechanical properties for solar heat collectors, AIP Adv. 10 (2020), 065016, https://doi.org/10.1063/5.0008786.

[28] A. Kusiak, J. Martan, J.-L. Battaglia, R. Daniel, Using pulsed and modulated photothermal radiometry to measure the thermal conductivity of thin films, Thermochim. Acta 556 (2013) 1–5, https://doi.org/10.1016/j.tca.2013.01.010.

[29] A. Kusiak, J.-L. Battaglia, S. Gomez, J.P. Manaud, Y. Lepetitcorps, CuO thin films thermal conductivity and interfacial thermal resistance estimation, Eur. Phys. J. Appl. Phys. 35 (2006) 17–27, https://doi.org/10.1051/epjap:2006064.

[30] C. Chassain, A. Kusiak, C. Gaborieau, Y. Anguy, N. Tran, C. Sabbione, M. Cyrille, J.-L. Battaglia, Film thicknesses influence on the interfacial thermal resistances within Ge-rich $Ge_2Sb_2Te_5$/$Ge_2Sb_2Te_5$ multilayers, Phys. Status Solidi (2023), 2300119, https://doi.org/10.1002/pssr.202300119.

[31] J.-L. Battaglia, A. Kusiak, V. Schick, A. Cappella, C. Wiemer, M. Longo, E. Varesi, Thermal characterization of the SiO_2–$Ge_2Sb_2Te_5$ interface from room temperature up to 400 ∘C, J. Appl. Phys. 107 (2010), 044314, https://doi.org/10.1063/1.3284084.

[32] H.R. Shanks, P.D. Maycock, P.H. Sidles, G.C. Danielson, Thermal conductivity of silicon from 300 to 1400K, Phys. Rev. 130 (1963) 1743, https://doi.org/10.1103/PhysRev.130.1743.

[33] M. Asheghi, K. Kurabayashi, R. Kasnavi, K. Goodson, Thermal conduction in doped single-crystal silicon films, J. Appl. Phys. 91 (2002) 5079–5088, https://doi.org/10.1063/1.1458057.

[34] A. Melhem, D. Meneses, C. Andreazza-Vignolle, T. Defforge, G. Gautier, A. Sauldubois, N. Semmar, Structural, optical and thermo-physical properties of mesoporous silicon layers: influence of substrate characteristics, J. Phys. Chem. C 121 (2017) 7821–7828, https://doi.org/10.1021/acs.jpcc.6b13101.

[35] J. Lascaud, T. Defforge, D. Certon, D. Valente, G. Gautier, In-depth porosity control of mesoporous silicon layers by an anodization current adjustment, J. Appl. Phys. 122 (2017), 214903, https://doi.org/10.1063/1.4997228.